International Journal of Precision Engineering and Manufacturing-Green Technology (2022) 9:1021–1034
https://doi.org/10.1007/s40684-021-00384-x

Online ISSN 2198-0810
Print ISSN 2288-6206

REGULAR PAPER

Speeding up Additive Manufacturing by Means of Forming for Sheet Components with Core Structures

Stephan Rosenthal[1] · Marlon Hahn[1] · A. Erman Tekkaya[1] · Sebastian Platt[2] · Stefan Kleszczynski[2] · Gerd Witt[2]

Received: 11 March 2021 / Revised: 2 July 2021 / Accepted: 16 August 2021 / Published online: 30 August 2021

Abstract
A new process combination route consisting of additive manufacturing (AM) with a subsequent forming operation is proposed. The process route has the opportunity to increase the efficiency of the AM process route up to 360%. Stainless steel 316L sheets with different core structures (similar to sandwich sheets) are produced by AM, characterized, and formed in a die bending operation. The bending characteristics of this novel semi-finished product can be accurately predicted in a numerical simulation. The new process route is discussed in detail and compared to conventional AM parts in terms of the production efficiency.

Keywords Additive manufacturing · Sheet forming · Efficient manufacturing · Hybrid process · Laser-powderbed fusion

1 Introduction and State of the Art

Sandwich sheets are commonly used due to their remarkable structural performance. High stiffness-to-weight ratio, high strength, and good crash performance are main characteristics, needed in aerospace, transportation, aviation, and automobile applications. The sandwich sheets are usually produced as flat or slightly curved panels. The forming of sandwich sheets into a different respectively final geometry is still a developing field of research, and for metallic sandwich sheets, offers the chance to produce curved parts with increased structural performance due to strain hardening.

Seong et al. [1] designed formable sheets with inner structures for lightweight applications with so called sheared dimple cores and brazed face sheets with the overall height H, bendable to a specific bending radius R, resulting in a relative bending radius $R/H = 3.33$. Core shear failure, face fracture, face buckling, and delamination were identified as the main failure modes [2]. Mohr [3] identified shear failure during U-bending as the dominant failure mode for draw bending of sandwich sheets and constructed design maps describing the required core shear strength as a function of the face sheet properties, the sandwich core thickness, and the drawing radius, based on a theoretical analysis. Formable sandwich sheets are usually produced by joining a metallic core structure to a metallic face sheet. The core can be designed as a periodically repeated metallic inner structure and is produced by blanking, punching, laser-cutting or stacking and gluing of corrugated foils [4].

An alternative method of producing cores for sandwich sheets is additive manufacturing (AM), specifically laser-powder-bed-fusion (PBF-LB/M) of metals, which is a constantly developing technology to produce customized parts with a high level of complexity and flexibility.

The combination of flexibility and complexity offers the benefit to achieve a high level of lightweight capabilities with the help of functional integration, load-adapted profiles and the use of intricate structures. These advantages come at the expense of low production rates, which makes AM currently inconvenient for the use in a broad application field. To overcome this challenge, one solution is the combination of AM with an efficient and productive manufacturing process – namely forming technology. In this paper, a new process combination is proposed. Semi-finished sheets are produced by AM, with intricate structures (similar to structured sandwich sheets), and formed to the final geometry in a subsequent forming operation (Fig. 1).

✉ Stephan Rosenthal
Stephan.Rosenthal@iul.tu-dortmund.de

[1] Institute of Forming Technology and Lightweight Components (IUL), TU Dortmund University, 44227 Dortmund, Germany

[2] Institut for Product Engineering (IPE), Chair of Manufacturing Technology, University of Duisburg-Essen, Lotharstraße 1, 47057 Duisburg, Germany

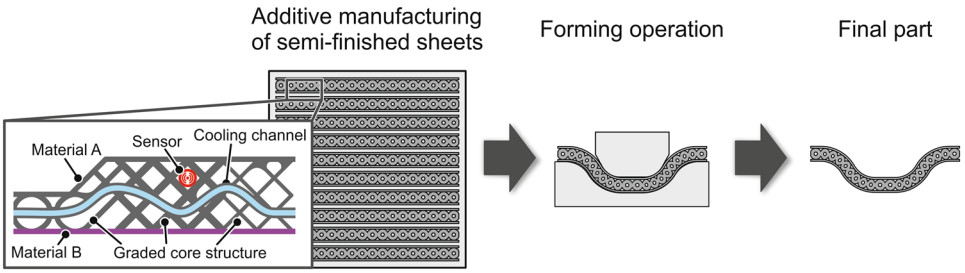

Fig. 1 Proposed process route. Additive manufacturing of semi-finished sheets with subsequent forming into the final geometry

The efficiency of this process is dependent on the whole process route – 1. Pre-processing, 2. Build-process (PBF-LB/M), 3. Post-processing – whose cost, production speed, and thus efficiency is still challenging [5]. Pre-processing contains the preparation of the CAD-part for the later AM-process. This includes the orientation of the workpiece to reduce the amount of support structures, creation of support structures, and nesting of the parts on the build-platform as well as the generation and calculation of the hatch vectors. Depending on the complexity of the produced parts, these steps can be time- and computation-intensive. The build-process includes the generation of the part, viz the layerwise distribution of the metal powder and the sequential melting and solidification using a laser. The post-processing step is necessary to remove the parts from the build chamber, remove the remaining powder and the support structure from the produced parts, as well as a final surface finish to reduce the process inherent surface roughness.

The build-up rates of current AM systems are still a major field of interest within research and industry [6]. Recent publications on increasing the efficiency in the PBF-LB/M process are mainly focused on increasing build-up rates by higher layer thicknesses or the use of multi-laser systems [7]. These multi-laser systems are already commercialized by TRUMPF GmbH, SLM- Solutions Group AG, eos GmbH, or DMG-Mori AG. Higher layer thicknesses of 250 µm are used by Shi et al. [8] to achieve a build-up rate of 9 mm^3/s by using comparatively high laser powers in the range of 400 W. However, the process quickly reaches its physical limits when using high laser powers. Staub et al. [9] showed that the use of high laser power favours keyhole melting and thus can reduce the density of the samples. A further increase can be achieved by an optimal usage of the available build-chamber volume. A fully used build-chamber results in fewer machine setup- and part removal operations, and hence in a more efficient manufacturing procedure.

It is important to consider not only the process itself but also the whole process route to increase the overall manufacturing efficiency. Strong et al. [10] point out that the additive manufacturing of metal parts can be integrated into existing process routes in order to achieve an increase in efficiency. Additively manufactured products should be finalized in traditional manufacturing shops by subsequent processes. Hybrid process routes consisting of AM and forming are currently limited to the production of functional elements on top of deep drawn sheets [11] and the deposition and forming of stiffness reinforcements [12]. Incremental forming of locally thickened sheets by AM to reduce thinning of the sheet during forming, or the manufacture of functional elements on the sheet before the forming operation is possible [13], as well as the use of wire-arc additive manufacturing of aluminium in a forging operation to reduce material waste [14]. Brandt et al. [15] give a comprehensive overview about the possibilities of AM to manufacture tools and dies for forming applications. A manufacturing concept to combine incremental sheet metal forming and laser-powder-deposition in one setup was invented by Hölker et al. [16]. This technology also enables the surface burnishing of AM parts.

The mentioned research activities are all focused so far on (a) The forming of sheet metal and AM in a subsequent step, or (b) The forming of simple, reinforced by AM, sheets or bulk material to the final shape, and (c) The usage of AM to produce tools and dies for forming applications. The production of advanced semi-finished sheets with complex inner structures to be used in a subsequent forming operation has not been investigated yet and is the topic of this paper with which a new hybrid process route is proposed. This approach mainly intends to drastically speed up the overall process time while still making use of the flexibility of the AM process.

2 New Hybrid Process Route

2.1 Process Route Description

The new process route is a combination of PBF-LB/M of complex shaped semi-finished sheets with internal structures, which are formed in a subsequent forming operation to their final geometry. As a result of the simple initial outer geometry and the subsequent forming to the final geometry, the efficiency of certain process route steps can be increased significantly. This offers several benefits, which will be discussed in the sections below. A comparison of both process routes is shown in Fig. 2. The process routes can be

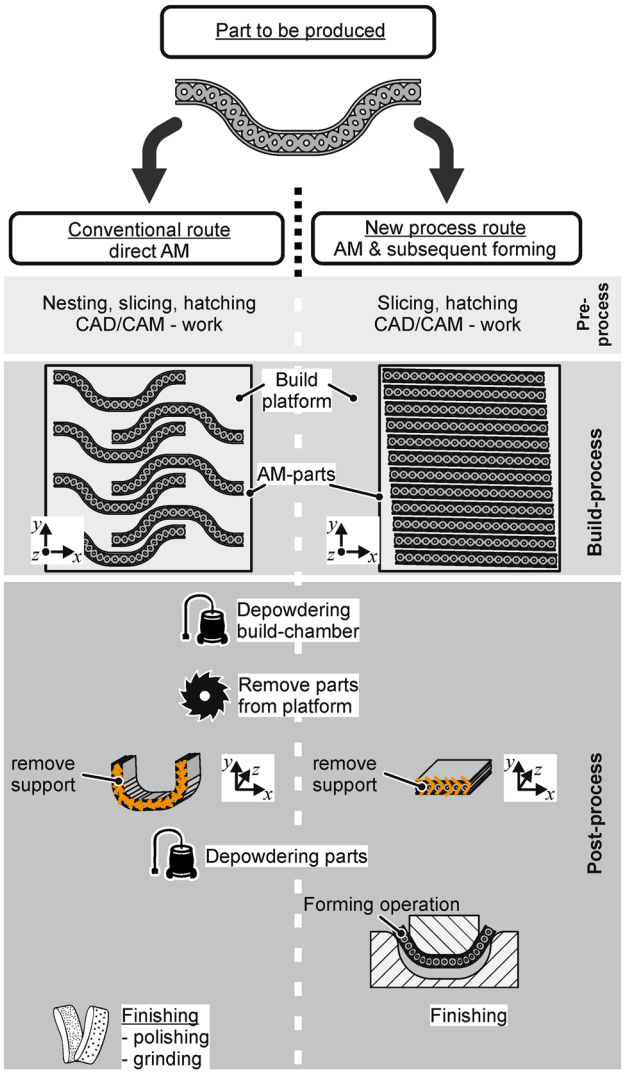

Fig. 2 New Process route: PBF-LB/M of semi-finished sheet and subsequent forming to the final geometry compared to the conventional AM-only route

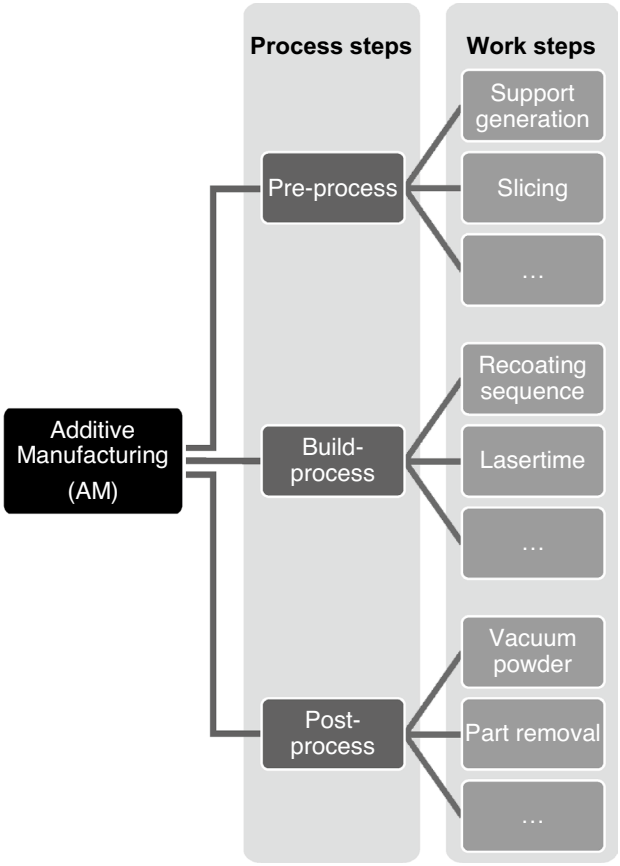

Fig. 3 Structuring of the additive manufacturing process for the efficiency evaluation

divided into three phases: pre-process, build-process, and post-process.

2.2 Efficiency Considerations

In the following, the efficiency of the AM process is investigated. Efficiency, in general, is defined as the ability to avoid wasting materials, energy, efforts, money and time in producing a desired result [17]. In the context of this paper, the efficiency is focused on the evaluation of the times that are needed to produce a specific part using only AM or the previously defined novel process combination of AM and subsequent forming. Both process routes are compared to each other.

The evaluation of the process efficiency is structured under the three main process steps that are typical in the AM process route: pre-process, build-process, and post-process, which can be further subdivided into individual work steps (Fig. 3). To investigate the efficiency of each process route, the times that are necessary to complete each step are investigated in detail. It is assumed that both process routes produce the same amount of parts. The time that is necessary to manufacture these parts will then be different for the two process routes and are the subject of the investigation. The evaluation of the process efficiency is based on the authors' experiences, measurements and corresponding calculations.

To ensure a transferable and machine-independent approach, a reference measure for the used building space needs to be defined. For this, the powder volume efficiency e_{PV} is defined. It is a measure that represents the available space provided by a AM-machine and is defined in Eq. (1) as the ratio between the sum of the volume of the produced parts V_{Sheet} divided by the available powder volume V_P.

$$e_{\mathrm{PV}} \overset{\mathrm{def}}{=} \frac{\sum V_{\mathrm{Sheet}}}{V_{\mathrm{P}}} \tag{1}$$

The available powder volume V_{P} is the volume of the powder that is needed to complete a full build-job and defined in Eq. (2).

$$V_{\mathrm{P}} = p \cdot q \cdot H_{\mathrm{Build}} \tag{2}$$

With p as the width and q as the length of the build chamber. For the special case that the height of the build chamber c of the used AM machine is equal to the build height H_{Build}, the powder volume efficiency will be equal to the build chamber efficiency. This case with $c = H_{\mathrm{Build}}$ will be investigated in the upcoming sections. In the following always the terminus powder volume efficiency is used Fig. 4.

2.2.1 Pre-Process

Pre-processing includes the preparation of the build-job i.e. support generation, nesting, slicing, and hatching. Those tasks, especially the nesting, can be time-consuming the more complex the part is, which gives plane parts an advantage. Flat parts can be stacked in the build-chamber in the most efficient way. Only a small gap of 1 mm in between the parts needs to be left to avoid a fusion of adjacent parts. This results in a build-chamber usage between 80 and 90%. Those flat sheets can be produced to be used in the combined process route of AM and subsequent forming. Equivalent parts can be produced directly in the final geometry using the conventional AM process route, whereas the possible complexity of the geometry needs to be taken into account. This is done by evaluating classes of geometries with different levels of complexity (Fig. 5a). The geometries are parametrized and varied through the parameters *a, b, H, R* and α with the constraint to have the same volume like the flat semi-finished sheets. The different geometries are arranged in the build chamber using an optimization algorithm to fit the maximum number of parts. Consequently, a strong dependency of the shape and the geometric characteristics is present, as well as a dependency of the size of the build platform. Figure 5b shows the resulting used build-chamber volumes for the evaluated geometries and the possible ranges of build-chamber usages that can be achieved. The used build-chamber volume decreases as the complexity of the parts increases and the ranges of possible build-chamber usages become smaller. There is no clear functional relationship between the final part geometry and the used build-chamber volume, which highlights the complexity and geometry-dependency of the packing problem, even for parts with a relatively low complexity. Still, there are some findings to be drawn and trends that can be concluded. An increased bounding box-ratio *a/b* leads to a more efficient usage of the build-chamber. Thus, shallow but long parts can be arranged more efficiently. This is what the new process route also pursues. The flat semi-finished sheets have the largest *a/b*-ratio and therefore can be arranged in the most efficient way possible. Therefore, the AM process is conducted in the most efficient way, meaning at the upper bound of the powder volume efficiency. Taking into account the shape of the final geometry, parts with small shoulder angles α can be arranged more efficiently than larger shoulder angles α or rectangular parts. This is a result of a better nestability. Depending on the final geometry, this can sum up to a more efficient build-chamber usage of up to 800% and will have a large influence on the amount of necessary build-jobs to produce the same amount of parts for both process routes.

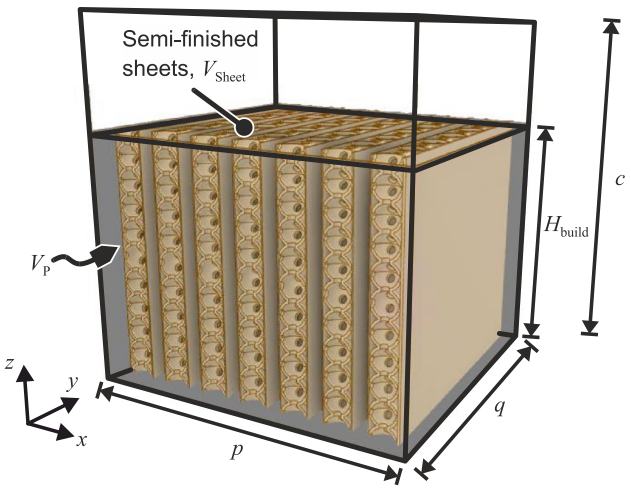

Fig. 4 Definition of the used powder volume

Furthermore, the process stability must be taken into account in determing the orientation of parts. In particular, part edges parallel to the recoater blade can reduce the process stability in the presence of superelevations. This could cause a collision between recoater blade and part. Therefore, parts are rotated around the vertical axis to achieve the shortest possible edge length parallel to the recoater blade. A rather complex geometry hinders a process-stable orientation by a multitude of differently oriented edges. Thus, the efficiency of the build-chamber is further reduced.

The times that are estimated during the pre-process of the considered build job (Fig. 5b, region 2) are shown in Fig. 6. The necessary tasks are the same for both process routes but need different times for completion. Though, if the support surface area is the same for both process routes, the support generation time is equal. The slicing time for the parts produced directly to the final geometry (conventional route) is larger. This is a result of a more complex geometry and therefore a higher discretizitaion of the surface model is necessary. Longer processing times can be attributed to the

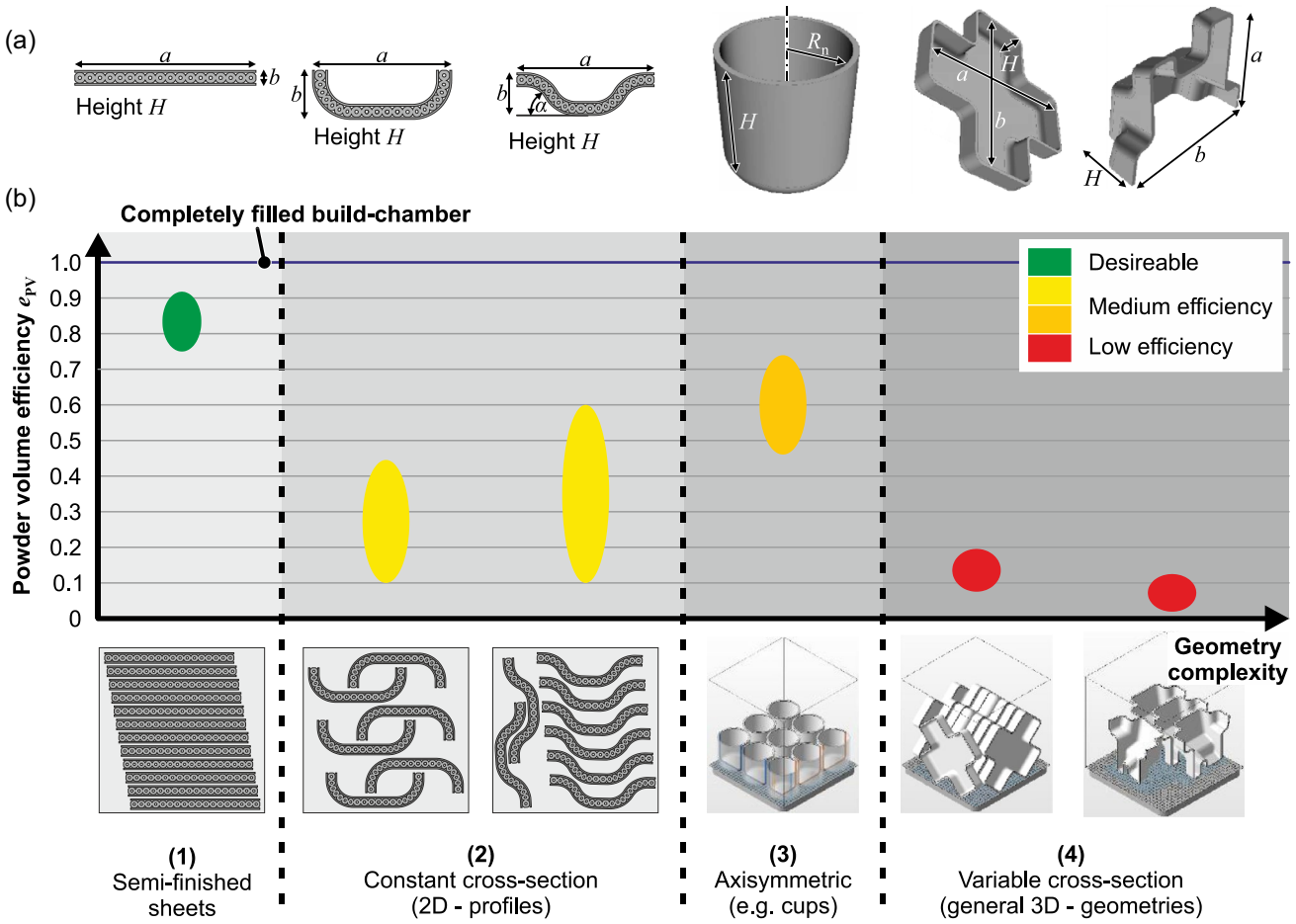

Fig. 5 **a** Classes of geometries of increasing complexity, **b** ranges for the powder volume efficiency $e_{PV.}$ for the classes of geometries. A value of $e_{PV.}=1$ would be equivalent to completely filling the build chamber with solid material. The volumes of the geometries are set equal to the volume of the semi-finished sheet

computation procedures behind the software tasks support generation, slicing and hatching. The estimated times are simply the processing times of the used software (rDesigner/Celos by DMG Mori). The time to perform each task by the user itself is incorporated in the user time. This results in a 54% faster processing time for the pre-processing of the new process route.

2.2.2 Build-Process

The build-process includes the local melting of the powder and the ensuing solidification as well as the recoating sequence in between the layers (Fig. 7a). The time for melting the powder is linear proportional to the exposure area of the parts. Skywritig can have an influence on the build speed [18] but is not considered in this study. Current machine systems homogenize the energy input by using the skywriting method. Here, the scan vectors of the laser beam are defined outside of the component contour in order to provide an area for acceleration and deceleration of the laser beam. The movement of the laser beam thus already takes place outside the actual part contour, but the actual laser energy is only applied in the area of the part. Thus, the melting of the material takes place at a constant speed and thus with a constant energy input. The additional scan vector length outside the part contour can thereby extend the exposure time of the part [18]. However, due to the layer-by-layer rotation of the scan vectors, the length of the scan vectors varies equally for both production routes and can be neglected. Therefore, the exposure or laser time for both process routes is the same. In the case of the production of semi-finished sheets with internal core structures, the exposure area is dependent on the relative density (actual volume divided by the bounding box volume) of the part itself and the amount of produced parts (Fig. 7b). The time of one recoating sequence is equal for each process and only dependent on the machine itself and the number of produced layers. To produce the same number of parts with the conventional process route, a second or third build-job is always

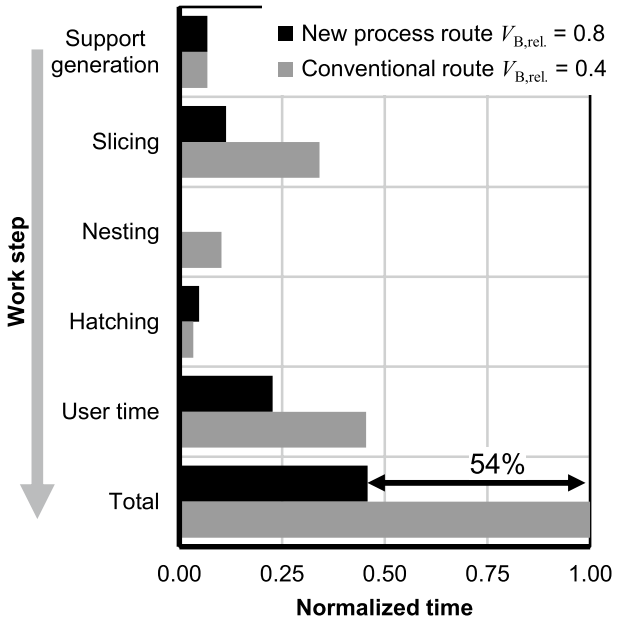

Fig. 6 Estimated times in the pre-processing step normalized by the total time needed to prepare the build-job in the conventional process route (Geometry: Fig. 5b, region 2)

necessary (depending on the final geometry). This results in a faster production speed using the combined process route and the time benefit sums up to 15%.

2.2.3 Post-Process

One of the most beneficial aspects of the new process route is the post-processing of the parts, as it offers high time saving potentials. Depowdering of the build-chamber takes less time, since less powder needs to be removed. To evaluate the differences between the conventional and the new process route, an additional time coefficient Ψ is generally defined as

$$\Psi \overset{\text{def}}{=} \frac{t_{\text{conv.}}}{t_{\text{new}}} \tag{3}$$

where $t_{\text{conv.}}$ is the time to finish a task for the conventional route and t_{new} is the time to finish a task for the process route of AM and forming. It shows the multiple of time that is necessary to finish a task using the conventional route compared to the combined process route. Specifically in case of the time to remove the powder, according to Eq. (3) the suction time-factor can be defined with the times $t_{\text{S,conv}}$ and $t_{\text{S,new}}$ as the times to vacuum the powder from the build-chamber as

$$t_{\text{S,conv.}} = \frac{\left(n_{bj} - 1\right) \cdot \left(A \cdot H_{\text{build}} - n_{\text{ppj}} \cdot V_{\text{part}}\right)}{\dot{V}_{\text{vac}}} + \frac{A \cdot H_{\text{build}} - \left[n_{\text{total}} - \left(n_{\text{bj}} - 1\right) \cdot n_{\text{ppj}}\right] \cdot V_{\text{part}}}{\dot{V}_{\text{vac}}} \tag{4}$$

for the conventional route. For the new process route, $n_{\text{bj}} = 1$ and $n_{\text{total}} = n_{\text{ppj}}$, $t_{\text{S,new}}$ can be derived as

$$t_{\text{S,new}} = \frac{A \cdot H_{\text{build}} - n_{\text{ppj}} \cdot V_{\text{part}}}{\dot{V}_{\text{vac}}} \tag{5}$$

where n_{bj} is the number of necessary build jobs, A is the build-platform area, H_{build} the build height, n_{ppj} the number

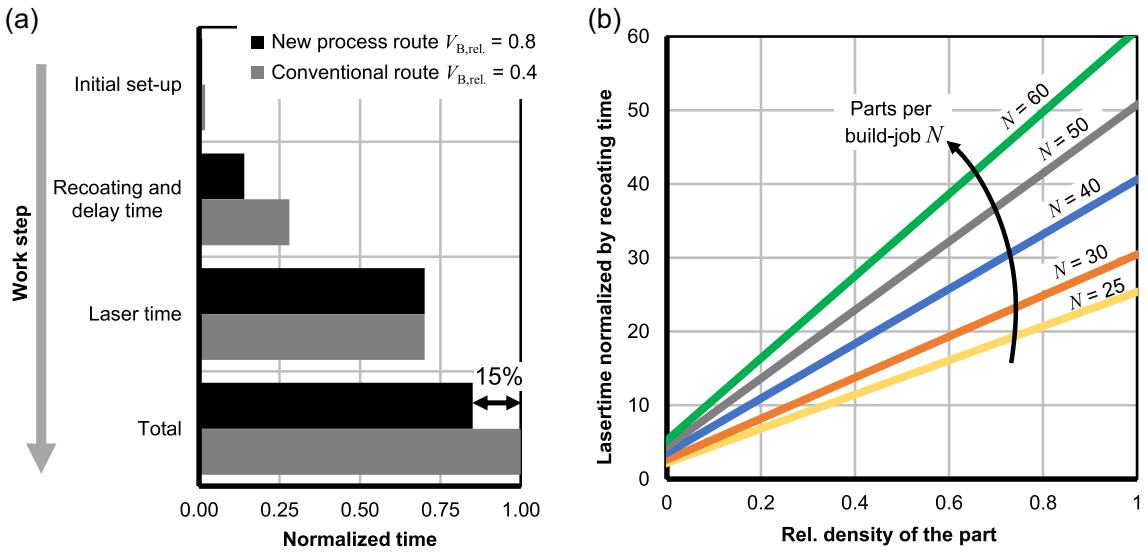

Fig. 7 **a** Estimated times in the build-process step normalized by the total time for a build-job in the conventional process route (Geometry: Fig. 5b, region 2), **b** dependency of the ratio of the laser- and recoating time on the relative density of the semi finished sheets

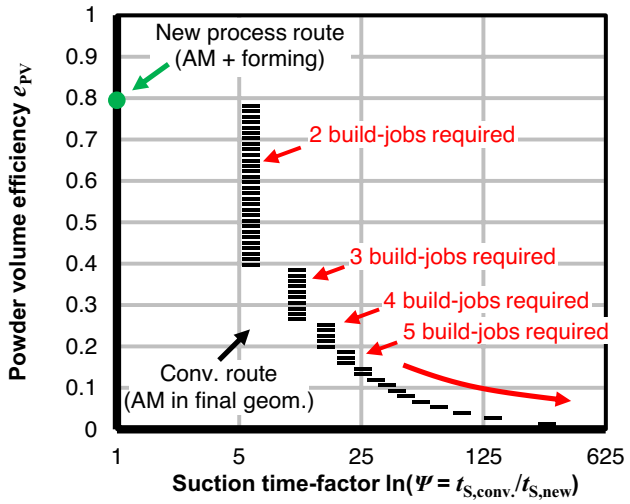

Fig. 8 Estimated increase in suction time with decreasing powder volume efficiency e_{PV}

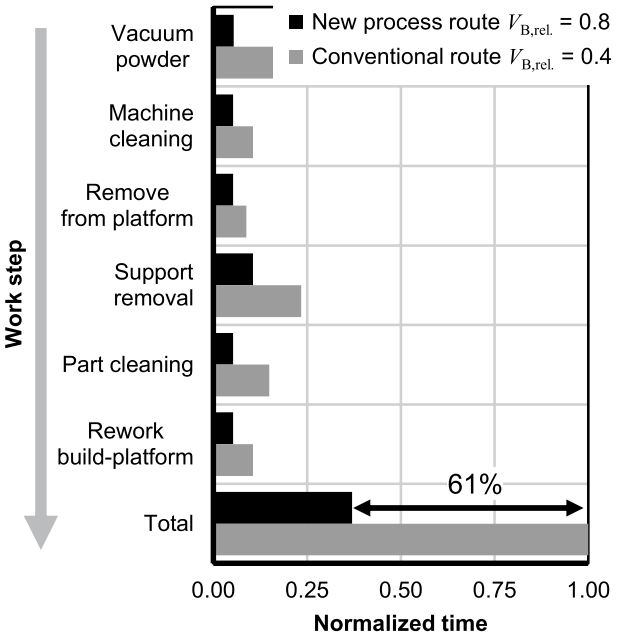

Fig. 9 Estimated times in the post-processing step normalized by the total time to process a job in the conventional process route (Geometry: Fig. 5b, region 2)

of parts that can be produced per build-job, V_{part} the volume of the produced part, n_{total} the total number of parts to be produced and V_{vac} is the flow rate of the vacuum. The first expression in Eq. (4) can be interpreted as the time to vacuum each build job with the highest possible parts packing density for the produced geometry and the second expression as the time for the last build job with the remaining parts to produce the required total number of parts. Already at one additional build job the required time to remove the powder with the vacuum increases by a factor of 5 (Fig. 8). With an increasing number of build jobs, the suction time factor Ψ increases overproportionally.

The estimated times for each work step are presented in Fig. 9. After vacuuming the build-chamber, it needs to be cleaned after every build-job to guarantee a safe processing for the next build-job. As already mentioned, it is always necessary to run at least one additional job in the conventional process route to manufacture the same amount of parts compared to the new route. Hence, at least twice as many cleaning setups are necessary.

The removal procedure of the parts from the build-platform is equal to the conventional route and requires a machining step, e.g. sawing or electrical discharge machining (EDM). Due to the higher number of build jobs of the conventional route, more building platforms have to be post-processed by sawing or EDM, which increases the setup and transfer times and therefore reduces the efficiency. A big advantage can be achieved when removing the support structure and depowdering the parts themselves. The amount of undercuts and unaligned powder-removal-holes is much larger than in the flat semi-finished sheets, which blocks the powder from being easily removed. Since the parts are flat, they can be condensed to a pile and processed at the same time, whereas the parts that are produced directly to their final shape need to be handled one by another, or the stacking is inefficient. The collective handling of the semi-finished sheets is beneficial for the powder removal from inner cavities as well. The parts can be handled in all process steps together. After the removal of the parts, the build-platforms, has to be prepared for the next build-job and the surface needs to be reworked. A good rule of thumb is that the post-processing steps usually take up to twice as long, since at least twice as much build-platforms need to be processed. All this gives a time benefit of 61% in the post-processing for the new process route for the considered case.

The subsequent forming operation of the semi-finished sheets will be taken into account in the next section, as it is an additional work step.

2.2.4 Overall Efficiency

Taking into account all previous process steps, a holistic view of the process efficiency of the new process route is now possible. The times to complete one process step are normalized by the time of the new process route, which gives a time factor Ψ (according to Eq. (3)) that indicates the multiple of time needed to produce the required parts in final geometry with the conventional process route (Fig. 10). The subsequent forming operation as well as final finishing step are added. Finishing of the parts includes a final preparation of the parts to achieve the final surface quality. The initial

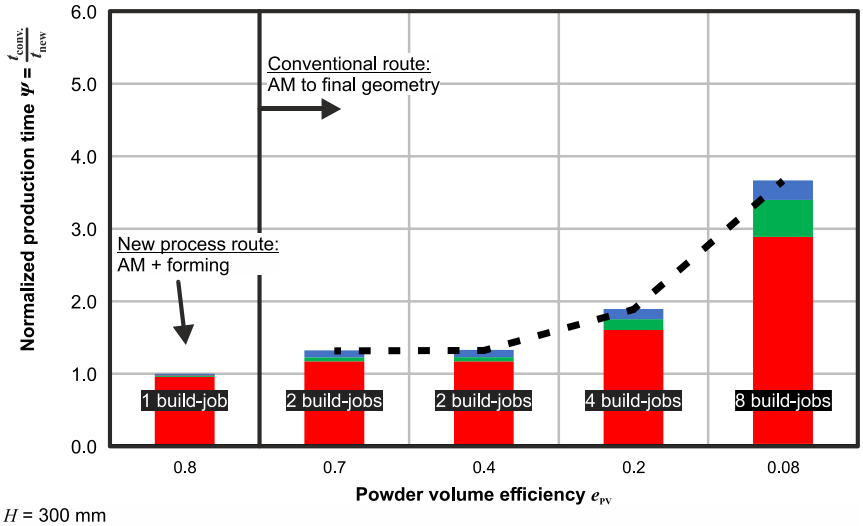

Build-height H = 300 mm

Finishing	0.025	0.097	0.098	0.140	0.271
Forming operation	0.001	0.000	0.000	0.000	0.000
Post-Processing	0.017	0.053	0.058	0.150	0.509
Build-job	0.951	1.160	1.159	1.587	2.855
Pre-Processing	0.006	0.012	0.012	0.017	0.032
Normalized time/part	1.000	1.316	1.321	1.887	3.661

Fig. 10 Resulting production time factor for the new and conventional process routes (cf. Figure 5)

roughness of the AM parts is relatively high and can or needs to be reduced by an additional surface finishing step, e.g. polishing or sand blasting. The new process combination has the advantage that during the forming operation, the surface is already being smoothened due to the frictional shear and normal forces generated by the relative tool movement in the workpiece area in contact with the tool. Measurements reveal that the mean surface roughness of the semi-finished sheets is $R_{z,nominal} = 37.5$ µm and the roughness of the parts that were subsequently formed is $R_{z,formed} = 27.75$ µm, which is a reduction of 26%.

The resulting efficiency increase of the new process route is at least higher by a factor of 1.31 and can rise up to 3.66 depending on the used powder volume efficiency (Fig. 10). It is important to notice, that the efficiency of the process is also dependent on the produced structure itself, since the geometry of the core influences the volume of the molten powder. It must be also kept in mind, that to produce the same amount of parts, the conventional route always needs at least one build-job more than the combined process route. Therefore, a lower bound for the normalized production time of the conventional route can be estimated ($\Psi = 1.4$), i.e. the conventional route takes at least 40% more time than the novel route.

In addition to the investigation of the production or time efficiency of the novel process route, the energy efficiency is also an important topic that needs to be addressed. A time efficient process does not always mean that it is energy efficient as well. Nowadays the energy efficiency of a process gains much more attention than in the past and is one of the most effective ways to contribute to a sustainable system. Due to the savings in labour- and time-consuming processing steps, the new process route may offer the chance to also further decrease the energy consumption of the process route. Therefore, in future works, the energy efficiency should be considered for the proposed novel process route as well.

3 Investigation of a Specific Structured Sheet Part

As shown in the previous section, the geometry of the produced parts has a significant influence on the process efficiency. According to Fig. 5, a hat-shaped geometry can be produced at relative build-chamber usages of 0.4. Thus, to produce the same amount of parts, a factor of two between the number of build-jobs for the new and conventional process route is necessary. This is a part configuration and a geometry whose forming characteristics will be investigated in the following, representing the abovementioned lower bound of efficiency increase.

3.1 Material Properties and Core Structures

The used material is a 316L stainless steel powder with a grain size of 15–45 µm. The parts are produced on a DMG Mori Lasertec 30 SLM machine. The process parameters are the standard settings delivered by DMG Mori. The material is tested in a standard tensile test in two manufacturing

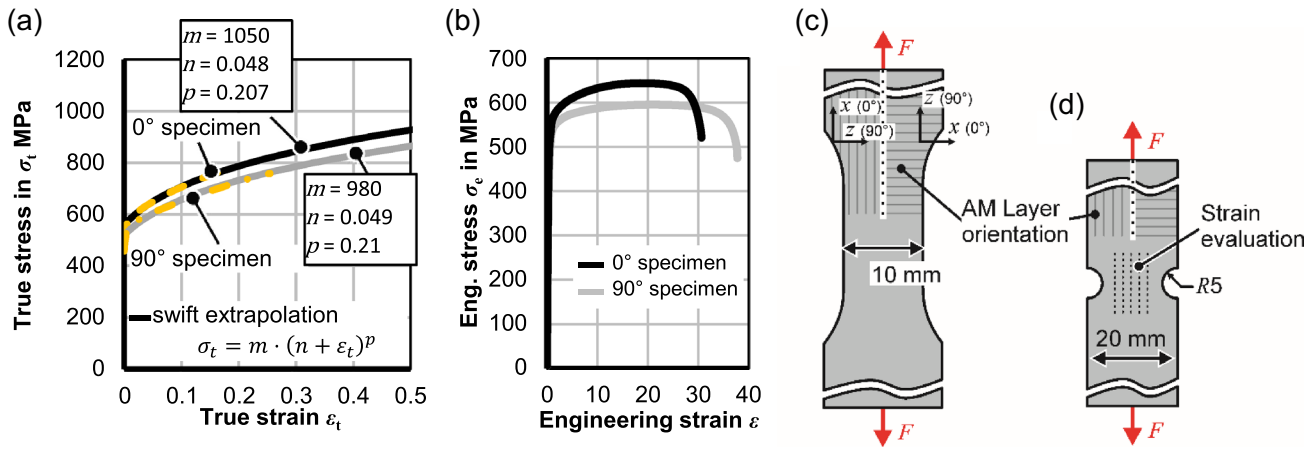

Fig. 11 Material properties of AM 316L (PBF-LB/M-Process, thickness of 2 mm), **a** true stress–strain diagram, **b** engineering stress–strain diagram, **c** specimen for standard tensile tests, **d** specimen for the evaluation of plane failure strain for forming limit curves [20]

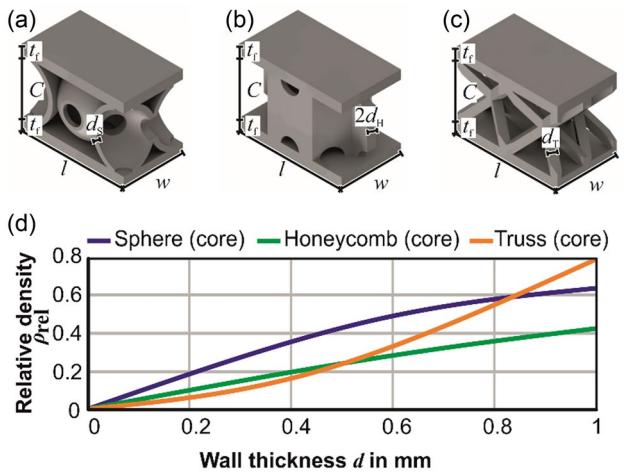

Fig. 12 Core structure unit cells **a** hexagonal spheres, **b** honeycomb, **c** truss lattice, t_f: face sheet thickness, C: core thickness, d_T; d_s; d_H: wall thickness(es) of the core, l: unit cell length, w: unit cell width, Overall height $H_c = 2t_f + C$, **d** relative densities of the core structures depending on the wall thickness d

directions (0°/90°) and stress–strain curves are recorded (Fig. 11). The Young's modulus is 200 GPa for both directions. The true stress–strain curves are extrapolated with the Swift hardening law in the plastic regime. To predict a possible failure during the bending of the sheets, notched tensile specimens as seen in Fig. 11d are performed. This specimen geometry represents the plane-strain deformation state, which corresponds to the deformation state in the tensile loaded area of the cross section of a bending part. The major strain is evaluated with digital image correlation at five lines along the specimen according to EN ISO 12004–2 standard [19]. The strains are evaluated at the last image before the fracture occurs. The mean failure strain that occurred in these tests is $\varepsilon_{fail} = 0.42$.

The core structures that are investigated in this study are depicted in Fig. 12 a-c and are designed to be manufacturable with AM. The holes in the core are necessary to be able to remove the remaining powder after the build process. The facesheet thickness is $t_f = 0.5$ mm = const. and the core height is $C = 3$ mm = const. for all structures. The wall thicknesses d_s, d_h, d_T can be varied to change the relative density ρ_{rel} of the core structures. The relative density is calculated as the real volume of the core divided by the fictive volume of the enclosed bounding box ($w \cdot l \cdot [2t_f + C] = \text{const.}$). The width $w = 3.25$ mm and length $l = 5.63$ mm are also held constant. The relation between relative density and wall thickness can be fitted through quadric functions, as can be seen from Fig. 12d. The trend in the slope of the relative density of the spherical and honeycomb structure show a degressive shape, whereas the truss structure shows a progressive relation between density and wall thickness.

The produced structures were originally designed to have the same equivalent unit cell shear stiffness (Eq. (6)) $G_{eq.} = 4500$ MPa with wall thicknesses $d_s = 0.25$ mm, $d_h = 0.49$ mm and $d_T = 0.4$ mm. For the calculation of the equivalent shear stiffness in Eq. (6), F stand for the shear force to elastically deform the unit cell by the increment dx, H_c is the overall height of the unit cell, and $A_c = l \cdot w$ is the cross sectional area.

$$G_{eq} = \frac{dF \cdot H_c}{dx \cdot A_c} \tag{6}$$

After manufacturing, the wall thicknesses are measured at multiple points in Fig. 13a-c and a deviation between the target and the actual mean value of the wall thicknesses of 13—17% is found. The original

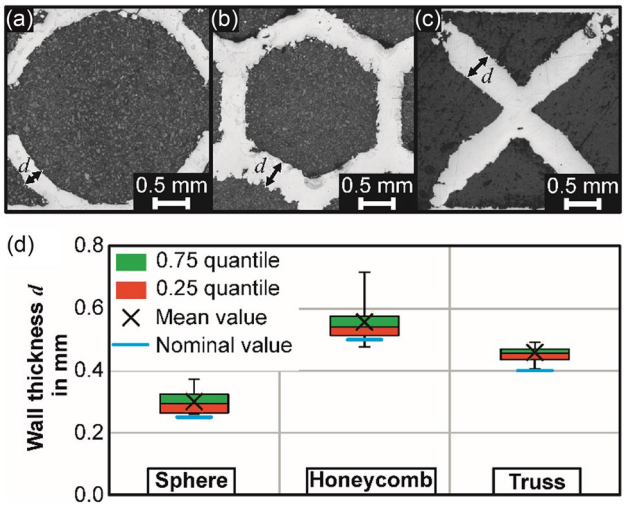

Fig. 13 Microscopic image of the unit cells **a** sphere, **b** honeycomb, **c** truss, **d** wall thickness measurements at multiple points

geometries are oversized compared to the nominal geometry from the CAD-model. Thus, any consideration with the nominal target geometry of the core structures would result in deviant solutions, so a properly corrected geometry should be taken into account based on the actual measurements.

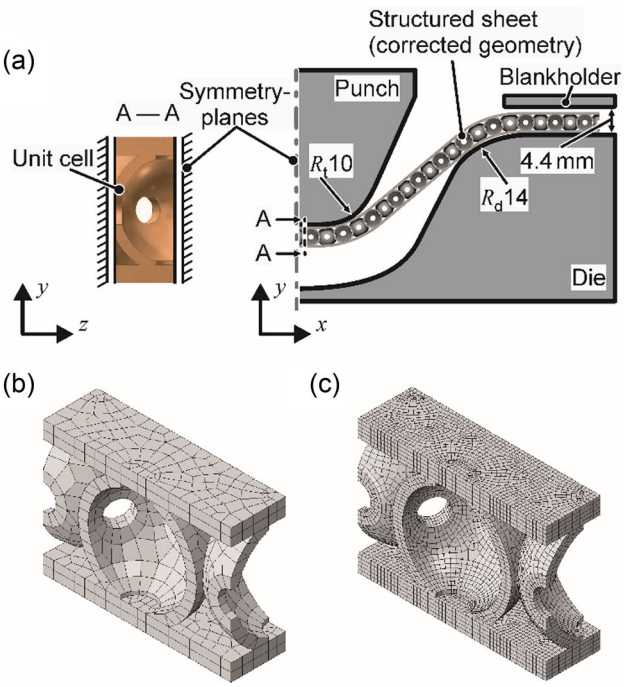

Fig. 14 Test setup for die-bending, **a** numerical setup, **b** coarse mesh of the whole model, **c** fine mesh for the submodel

3.1.1 Forming Behavior of the Structured Sheets

To deeply investigate the bending behavior of the novel sheet structures, numerical simulations are performed using Abaqus 2019 standard and compared with experiments. The setup is shown in Fig. 14. Due to the fine and intricate geometry of the core structure, the overall bending simulation is performed using hexahedral volume elements (C3D8I) with a mean element length of 0.28 mm (Fig. 14b). The friction coefficient $\mu = 0.15$ was determined experimentally in a strip drawing test [21] and self-contact is activated for the whole structured sheet.

To analyse the stresses and strains during the forming operation locally, a submodel with a higher mesh density and smaller mean element length of 0.08 mm is utilized to accurately represent the areas of interest (Fig. 14c). In the submodel, the local boundary conditions are automatically extracted from the overall model by the software [22].

For the experiments, the semi-finished sheets are produced with an angle to the build platform of 10° to guarantee a stable process. Support structures are only necessary at the bottom of the part to stabilize the part and ensure heat transfer (Fig. 15a). The semi-finished sheets are shown in Fig. 15b, with the dimensions being 170 mm x 30 mm x 4 mm.

The dominant loads in a bending operation result in plane strain. Therefore, the plastic strains along the bending line, which complies with the element-local x-direction (ε_{11}) are focused.

Figure 16 shows resulting parts from the numerical bending simulation. The different structures are bent into a hat

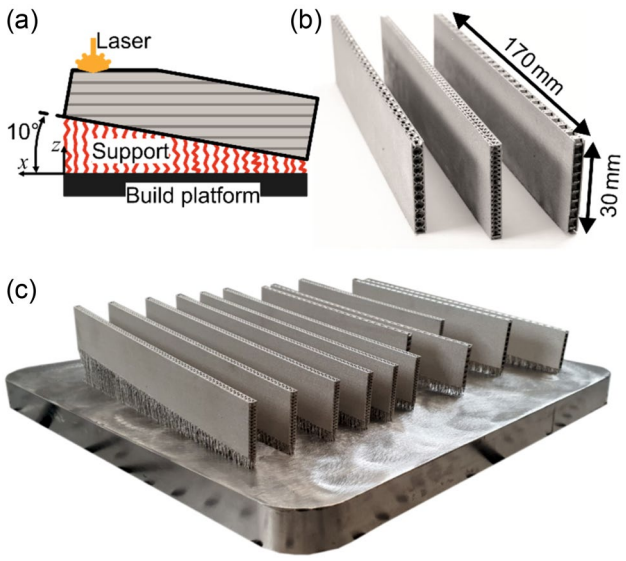

Fig. 15 Semi-finished AM sheets, **a** build orientation, **b** finished sheets with core structures, **c** specimen on the build plattform

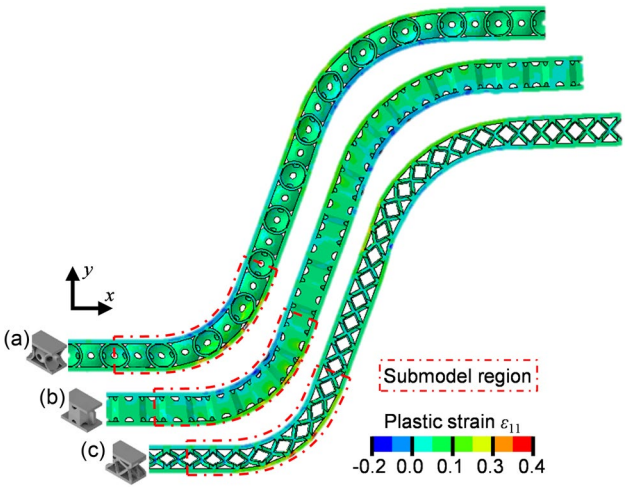

Fig. 16 Results from the numerical bending simulation with a punch radius of 10 mm, **a** spherical structure, **b** honeycomb structure, **c** truss structure

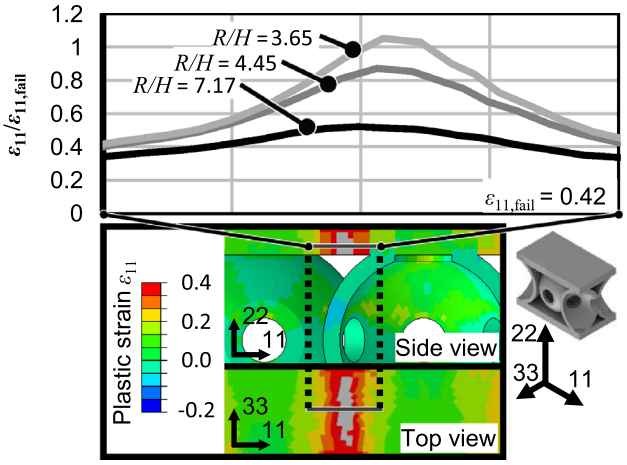

Fig. 18 Local strain distribution at critical location of the sheet with the spherical structure. *H*: Overall thickness of the sheet ($H=2t_t+C$), *R*: Current radius of the sheet during the forming operation

shape. This shape allows for a calibrating force at the end of the forming operation. A further increase in strain hardening can be achieved by the use of a higher blank holder force. The results show that the forming of the structures can be achieved up to a tool radius of $R_t = 10$ mm. The strain distributions in Fig. 16 show rather small strains in the core itself. The maximum strains are reached at the bottom of the die in the outer facesheet and show a dependence on the underlying core structure Figs. 17, 18, 19. The distance between the attachment points of the core and the face sheet influences the strain distribution and thus the maximum strain. The largest strains are visible in the sheet with the spherical core structure (Fig. 16a, and Fig. 19) with $\varepsilon_{11} > 0.40$, which has the smallest gap between the attachment points. The other structures show smaller strains in this region (Fig. 16b, c, and Fig. 19). The spherical structure and the truss structure,

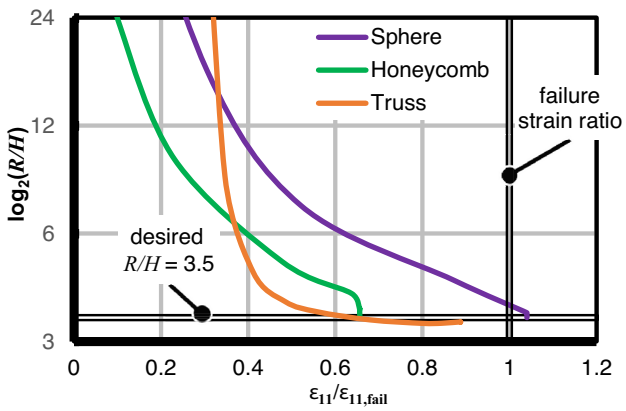

Fig. 17 Bending ratios and strain evolution of the unit cells obtained from the numerical simulation

Fig. 16a and c, yield a larger thinning of the whole sheet as a result of a smaller structural stiffness and strength in thickness direction compared to the honeycomb structure.

To take a closer look at the critical areas of the forming operation in the area at the bottom of the die, the submodels for all structures are considered. Since no severe distortion of the core or buckling was observed, the dominant failure mechanism is strain concentration, i.e. necking (similar to formability considerations of conventional sheet blanks). From the plane strain tensile tests it is known that the maximum failure strain is $\varepsilon_{fail} = 0.42$. The strain evolution during the bending operation can be seen in Fig. 17. The decreasing ratio of the current bending radius to the total sheet thickness, *R/H,* depicts the evolution of the bending operation over the failure-normalized strain. As in conventional bending, with decreasing *R/H,* this strain ratio naturally increases, meaning that failure comes closer the smaller the radius gets. However, different courses apply for the different cores regarding the mentioned relation. A desired bending ratio of $R/H = 3.5$, for example, is reached by the honeycomb and truss structure sheets without reaching the failure strain. But the sheet with the spherical structure seems to reach strains above the theoretical (or characterized) failure, indicating a potential face-sheet crack in the experiments.

The potential failure of the face sheet of the spherical structure can be investigated further by looking at Fig. 18. The local strain concentration occurs in the middle between two spheres, whose connections to the face sheet act like almost fixed supports, and is reached at $R/H = 3.65$.

The force–displacement curves of the experiment and the simulation are compared and demonstrate an accurate agreement (Fig. 19a-c). The experiments with a tool radius of $R_t = 10$ mm also show a failure-free forming of the sheets, except for the sheet with the spherical structure.

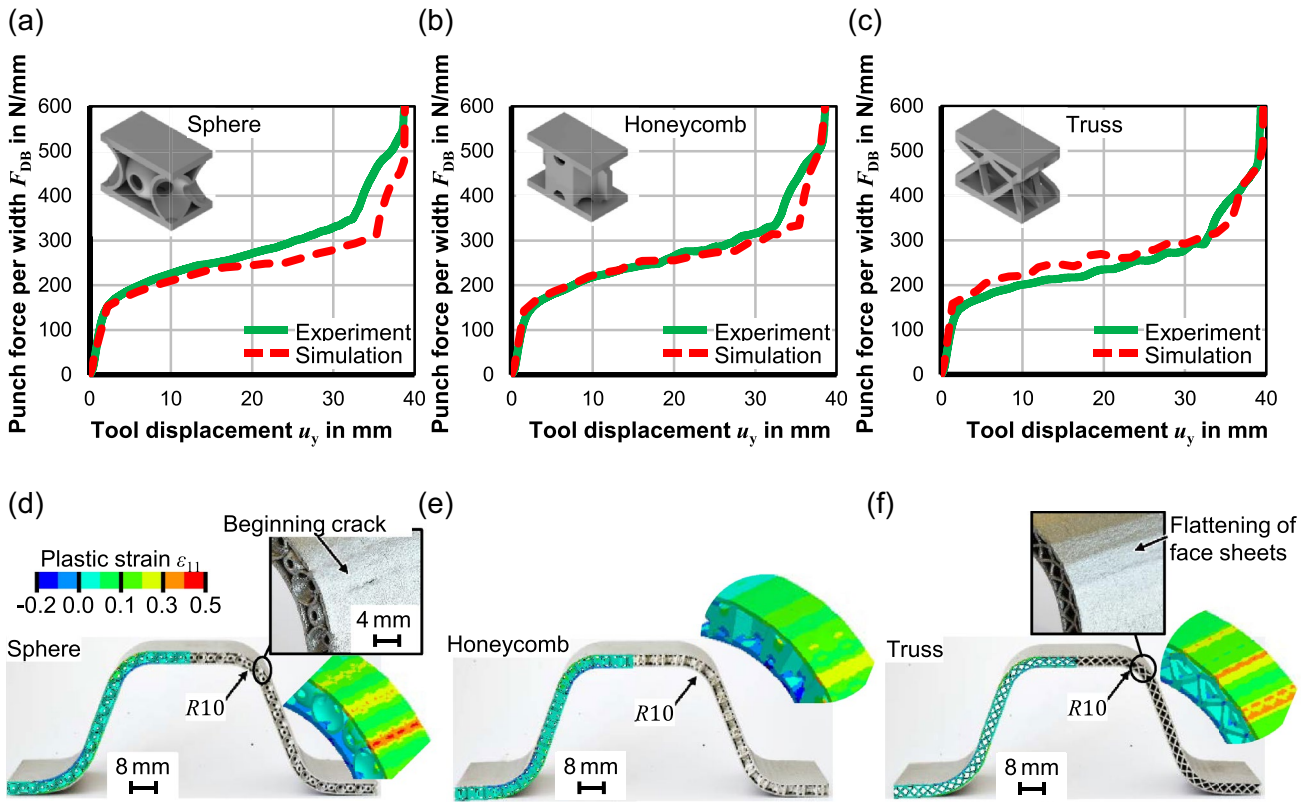

Fig. 19 Bending experiments, **a–c** Experiment vs. numerical simulation, **d–f** Formed part and detail of numerical simulation submodel

Experiments with larger tool radii were successful for all structures. The sheet with the spherical structure fails under strain concentration occurring in the face sheet (Fig. 19d). A beginning crack is visible after the forming operation. The region of the crack fits accurately with the prediction of the numerical simulation. Sheets with the other structures reveal a strain concentration in the same area but with a lower magnitude and no visible crack (honeycomb $\varepsilon_{11} = 0.30$, truss $\varepsilon_{11} = 0.36$). Neither core shear failure nor buckling as also predicted numerically. The results of the truss structure show that a buckling-mode occurs at a tool displacement of $u_y = 20$ mm. However, as the bending process continues, the induced wrinkle in the face sheet is straightened during unbending and is not present anymore after the completed forming process (Fig. 19f). Next to that, the face sheet exhibits a flattened pattern after the forming operation. This is a result of the unsupported face sheets in a comparatively large area over the core. Tensile stresses in the face sheet cause a straightening of these unsupported areas along the bending line.

The sheet with the honeycomb structure can be formed without defects. This structure offers a good support for the face sheets over a large area. Comparing the strains in the face sheets of all structures, a correlation between the shape of the core structure and the face sheet strains is derivable. With an increased gap between the connection points, the tensile strains in the face sheets are reduced. Experiments with a U-bending process and a blankholder show qualitatively very similar results (not presented in this paper), but the strains are of a higher magnitude in this case, since the drawing and the unbending after the drawing radius result in higher forming forces.

4 Conclusion and Outlook

A new process route combining additive manufacturing (PBF-LB/M) and a subsequent forming operation to reach the final geometry is presented. The new process route opens the opportunity to increase the efficiency of the process route by at least 40% and up to 680% compared to pure AM. A methodology is presented to evaluate the efficiency of the new process route. The critical aspect to increase the overall efficiency is an increased usage of the available powder volume to 80%, which appears to be the upper bound of the process. As a result, the material can be used in the most efficient way and leads to less material waste, especially in high performance applications where the powder in each batch is only used once. Three core structures for the novel sheets are investigated regarding their formability in a die

bending operation. Experiments and numerical simulations reveal an accurate agreement. The dominant failure mode is strain concentration in the face sheet due to tensile strains. This can be predicted accurately with the help of plane strain tensile test data in the numerical simulations. The core structure stays intact in each case.

Further investigations will focus on the dependency of the gap between the attachment points and the face sheet failure, along with an analytical description. In addition, the increase in the structural enhancement through the strain hardening during forming will be identified quantitatively. The geometry of the core structure can be optimized by geometric or topology optimization which offers high potentials, especially in combination with additive manufacturing. To even further increase the performance of the novel sheets, AM can be used to integrate functions into the core of the sheet, like cooling channels or sensors.

Acknowledgements This paper is based on results of the project forming of additively manufactured sandwich sheets with optimized core structures (Project number 317137194), which is kindly supported by the German Research Foundation (DFG). The authors also thank Pia Greiten (student) for her contribution in the field of the efficiency analysis.

Funding Open Access funding enabled and organized by Projekt DEAL.

Declarations

Conflict of interest On behalf of all authors, the corresponding author states that there is no conflict of interest.

References

1. Seong, D. Y., Jung, C. G., Yang, D. Y., Kim, J. H., Chung, W. J., & Lee, M. Y. (2010). Bendable metallic sandwich plates with a sheared dimple core. *Scripta Materialia*. https://doi.org/10.1016/j.scriptamat.2010.03.022
2. Seong, D. Y., Jung, C. G., Yang, D. Y., Ahn, J., Na, S. J., Chung, W. J., & Kim, J. H. (2010). Analysis of core shear stress in welded deformable sandwich plates to prevent de-bonding failure during U-bending. *Journal of Materials Processing Technology*. https://doi.org/10.1016/j.jmatprotec.2010.02.026
3. Mohr, D. (2005). On the role of shear strength in sandwich sheet forming. *International Journal of Solids and Structures*. https://doi.org/10.1016/j.ijsolstr.2004.07.012
4. Ahn, D.-G. (2015). Research trends of metallic sandwich plates with single layer periodically repeated metallic inner structures (PRMIS) - focused on design, manufacturing and formability. *International Journal of Precision Engineering and Manufacturing-Green Technology*. https://doi.org/10.1007/s40684-015-0046-3
5. Despeisse, M., Ford, S. (2015). The role of additive manufacturing in improving resource efficiency and sustainability. In: Umeda, S., Nakano, M., Mizuyama, H., Hibino, H., Kiritsis, D., Cieminski, G. von (Eds.) Advances in production management systems: Innovative production management towards sustainable growth. IFIP WG 5.7 International Conference, APMS 2015, Tokyo, Japan, September 7–9, 2015, Proceedings, Part II, vol. 460. IFIP Advances in Information and Communication Technology, vol. 460, 1st edn., pp. 129–136. Springer International Publishing, Cham, s.l.
6. Gutowski, T., Jiang, S., Cooper, D., Corman, G., Hausmann, M., Manson, J.-A., Schudeleit, T., Wegener, K., Sabelle, M., Ramos-Grez, J., & Sekulic, D. P. (2017). Note on the rate and energy efficiency limits for additive manufacturing. *Journal of Industrial Ecology*. https://doi.org/10.1111/jiec.12664
7. Poprawe, R., Hinke, C., Meiners, W., Schrage, J., Bremen, S., Merkt, S. (2015). SLM production systems: Recent developments in process development, machine concepts and component design. In: Brecher, C. (Ed.) Advances in production technology. Lecture Notes in Production Engineering, pp. 49–65. Springer Open, Cham, Heidelberg, New York, Dordrecht, London
8. Shi, W., Wang, P., Liu, Y., Hou, Y., & Han, G. (2020). Properties of 316L formed by a 400 W power laser selective laser melting with 250 μm layer thickness. *Powder Technology*. https://doi.org/10.1016/j.powtec.2019.09.059
9. Staub, A., Spierings, A. B., & Wegener, K. (2019). Correlation of meltpool characteristics and residual stresses at high laser intensity for metal lpbf process. *Advances in Materials and Processing Technologies*. https://doi.org/10.1080/2374068X.2018.1535643
10. Strong, D., Sirichakwal, I., Manogharan, G. P., & Wakefield, T. (2017). Current state and potential of additive – hybrid manufacturing for metal parts. *Rapid Prototyping Journal*. https://doi.org/10.1108/RPJ-04-2016-0065
11. Merklein, M., Junker, D., Schaub, A., & Neubauer, F. (2016). Hybrid additive manufacturing technologies – an analysis regarding potentials and applications. *Physics Procedia*. https://doi.org/10.1016/j.phpro.2016.08.057
12. Bambach, M., Sviridov, A., Weisheit, A., & Schleifenbaum, J. (2017). Case studies on local reinforcement of sheet metal components by laser additive manufacturing. *Metals*. https://doi.org/10.3390/met7040113
13. Ambrogio, G., Gagliardi, F., Muzzupappa, M., & Filice, L. (2019). Additive-incremental forming hybrid manufacturing technique to improve customised part performance. *Journal of Manufacturing Processes*. https://doi.org/10.1016/j.jmapro.2018.12.008
14. Silva, C. M. A., Bragança, I. M. F., Cabrita, A., Quintino, L., & Martins, P. A. F. (2017). Formability of a wire arc deposited aluminium alloy. *Journal of the Brazilian Society of Mechanical Sciences and Engineering*. https://doi.org/10.1007/s40430-017-0864-z
15. Brandt, M., R. Hölker-Jäger, A.E. Tekkaya (Eds.) (2017). Laser additive manufacturing. Materials, design, technologies, and applications. Woodhead Publishing series in electronic and optical materials, number 88. Elsevier/Woodhead Publishing Woodhead Publishing is an imprint of Elsevier, Amsterdam, Boston

16. Hölker, R., Khalifa, N.B., Tekkaya, A.E.: Method and device for the combined production of components by means of incremental sheet forming and additive methods in one clamping setup Patent WO2016045651A1
17. Longman Dictionary of Contemporary English: "Efficiency". https://www.ldoceonline.com/dictionary/efficiency. Accessed 1 Feb 2020
18. Moylan, S., Slotwinski, J., Cooke, A., Jurrens, K., & Donmez, M. A. (2014). An additive manufacturing test artifact. *Journal of Research of thr National Institute of Standards and Technology*. https://doi.org/10.6028/jres.119.017
19. DIN EN ISO 12004-2:2009-02, Metallische Werkstoffe_- Bleche und Bänder_- Bestimmung der Grenzformänderungskurve_- Teil_2: Bestimmung von Grenzformänderungskurven im Labor (ISO_12004–2:2008); Deutsche Fassung EN_ISO_12004–2:2008. Beuth Verlag GmbH, Berlin
20. Chen, H., Staupendahl, D., Hiegemann, L., & Tekkaya, A. E. (2017). Increasing the formability of ferritic stainless steel tube by granular medium-based hot forming. *Journal of Physics Conference Series*. https://doi.org/10.1088/1742-6596/896/1/012009
21. Doege, E., Witthüser, K.-P., & Grahnert, R. (1981). Untersuchung der Reibungsverhältnisse beim Tiefziehen. In W. Bunk, J. Hansen, & M. Geyer (Eds.), *Tribologie Reibung Verschleiß Schmierung* (pp. 551–575). Springer.
22. Dassault Systems: Abaqus (2020) user manual. Abaqus > Abaqus/CAE > Modeling techniques > Submodeling (2019)

Stephan Rosenthal graduated with a B.Sc. and M.Sc. in 2016 from Hamburg University of Technology. Since 2017 he is working as a researcher at the IUL at the TU Dortmund University. He is an expert in additive manufacturing technologies for applications in forming technology and is currently working towards his Ph.D.

Marlon Hahn received his M.Sc. degree in industrial engineering from TU Dortmund University in 2014 and is since then working as a researcher at the IUL in different forming-related areas. He currently serves as the head of the department of non-conventional processes at the IUL.

A. Erman Tekkaya received his B.Sc. (1979) and M.Sc. (1980) degrees from the Mechanical Engineering Department, Middle East Technical University (METU), Ankara/Turkey. In 1985 he obtained a Ph.D. at the Institute of Forming Technology, University of Stuttgart, Germany. Since 2007, he is the Professor and Head of Institute of the IUL at the TU Dortmund University, Germany. He is a member of several forming technology expert committees and he has contributed over 800 publications in journals and conference proceedings.

Sebastian Platt Ph.D. student at the Chair of Manufacturing Technology of the University Duisburg-Essen, Germany. His research interests include the in- and extrinsic influencing of the PBF-LB/M process.

Stefan Kleszczynski Senior researcher at the Chair of Manufacturing Technology of the University Duisburg-Essen, Germany. His research interests include additive manufacturing of bulk metallic glasses and increasing the reproducibility of the PBF-LB/M process.

Gerd Witt Professor of Manufacturing Technology at the University Duisburg-Essen, Germany. His research interests include further developing the technology and the process chain of additive manufacturing and qualifying it for series production as well as opening new fields of application.